frontiers | Frontiers in Photonics

TYPE Brief Research Report
PUBLISHED 05 August 2024
DOI 10.3389/fphot.2024.1416347

Check for updates

OPEN ACCESS

EDITED BY
Maciej Trusiak,
Warsaw University of Technology, Poland

REVIEWED BY
Michał Józwik,
Warsaw University of Technology, Poland
Adam Styk,
Warsaw University of Technology, Poland

*CORRESPONDENCE
Mostafa Agour,
agour@bias.de

RECEIVED 12 April 2024
ACCEPTED 15 July 2024
PUBLISHED 05 August 2024

CITATION
Agour M, Thiemicke F, Müller AF, Bergmann RB and Falldorf C (2024) Lensless multi-spectral holographic interferometry for optical inspection.
Front. Photonics 5:1416347.
doi: 10.3389/fphot.2024.1416347

Lensless multi-spectral holographic interferometry for optical inspection

Mostafa Agour[1,2]*, Fabian Thiemicke[1], André F. Müller[1], Ralf B. Bergmann[1,3] and Claas Falldorf[1]

[1]BIAS-Bremer Institut für angewandte Strahltechnik, Bremen, Germany, [2]Physics Department, Faculty of Science, Aswan University, Aswan, Egypt, [3]MAPEX Center for Materials and Processes and Faculty of Physics and Electrical Engineering, University of Bremen, Bremen, Germany

We explore the principles, implementation details, and performance characteristics of a lensless multi-spectral digital holographic sensor and demonstrate its potential for quality assurance in semiconductor manufacturing. The method is based on capturing multi-spectral digital holograms, which are subsequently utilized to evaluate the shape of a reflective test object. It allows for a compact setup satisfying high demands regarding robustness against mechanical vibrations and thus overcomes limitations associated with conventional optical inspection setups associated with lens-based white light interferometry. Additionally, the tunable laser source enhances the versatility of the system and enables adaptation to various sample characteristics. Experimental results based on a wafer test specimen demonstrate the effectiveness of the method. The axial resolution of the sensor is $\pm$ 2.5 nm, corresponding to 1σ.

KEYWORDS

white light interferometry, digital holography, optical inspection, shape measurement, wafer inspection

1 Introduction

In the fast-evolving landscape of the chip industry, the pursuit of quality is paramount to ensure the reliability and functionality of semiconductor devices (Bechtler and Velidandla, 2003; Krauter et al., 2017). Quality inspection, particularly at the wafer level, is a critical task that demands axial precision in the nanometer range across an extent of several tenths of microns (Colonna de Lega and De Groot, 2005; Strapacova et al., 2017).

Established methods for optical inspection (Osten, 2018), such as white light interferometry (WLI) and confocal microscopy, have been instrumental in achieving high resolution (De Groot and Deck, 1995; Vogel et al., 2011). However, their application in in-production or in-line quality inspection has been hindered by severe challenges (Agour et al., 2015). Traditional optical inspection methods face practical limitations due to their sensitivity to mechanical disturbances during the acquisition process (Bergmann et al., 2021). In addition, they are subject to other distortions from various sources, including optical system imperfections (such as misalignment and focusing errors), dust and reflections (Migukin et al., 2013). Moreover, the sophisticated imaging systems associated with these methods are not only expensive but also heavy, rendering them inflexible and slow.

This paper introduces an innovative approach aimed at overcoming these challenges by using a lensless digital holographic sensor paired with a wavelength-tunable laser as the light source. This approach is based on our recently developed fullfield lensless acquisition of spectral holograms or Flash-WLI (Falldorf et al., 2023). Unlike traditional systems, this configuration captures multi-spectral digital holograms, which are subsequently utilized to evaluate the shape of a reflective specimen under test. The lensless digital holographic sensor brings a paradigm shift in wafer-level inspection, overcoming the limitations towards robustness and flexibility of conventional white-light interferometers. Its compact design eliminates the need for complex imaging systems, providing flexibility and ease of integration into existing production lines. Furthermore, the sensor's ability to operate in a mechanically less constrained environment enhances its suitability for in-line applications. The wavelength tunability of the laser source adds an extra degree of freedom to the versatility of the system, allowing adaptability to different specimen characteristics.

In this publication, we delve into the principles, implementation, and performance of the lensless digital holographic sensor in the context of in-line wafer-level inspection. We present experimental results based on a wafer test specimen, showcasing its efficacy in providing precise, nanoscale-resolution measurements. The proposed method not only addresses the shortcomings of current inspection techniques but also paves the way for enhanced efficiency, cost-effectiveness, and adaptability in the dynamic realm of chip manufacturing.

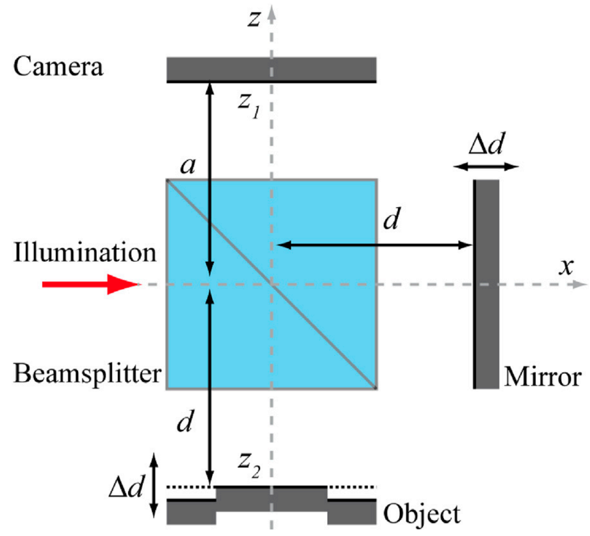

FIGURE 1
The concept of Flash-WLI: The setup is a simple Michelson type interferometer that enables the recording of digital holograms of the object under test. The camera sits at a distance a from the beam splitter cube in the recording plane z_1. Both, the reference mirror and the object plane z_2 have the same distance d from the cube. The idea is to record multiple holograms with different wavelengths of illumination. Based on these multi-spectral holograms, a coherence scan is performed through variation of d, and thus z_2, by Δd. The results are similar to those of white light interferometry. However, in the case of Flash-WLI, only a single set of multi-spectral holograms is needed, because the scan is performed numerically by calculation of the coherence function across various depth $z_2 = -(a + d + \Delta d)$ without any actual movement of the mirror.

2 Methods

Figure 1 shows the basic setup of Flash-WLI (Falldorf et al., 2023). It represents a Michelson type interferometer with the reflective specimen in one of the interferometer arms. Let us denote the recorded intensity in the sensor domain by (Schnars et al., 2015):

$$I_n(x,z_1) = |u_n(x,z_1)|^2 + |r_n(x,z_1)|^2 + u_n(x,z_1)\cdot r_n^*(x,z_1) + u_n^*(x,z_1)\cdot r_n(x,z_1). \tag{1}$$

In Equation 1 u_n and r_n denote object and reference wave respectively, x is a coordinate in the sensor plane located at z_1, and n refers to the measurement number with wavelength λ_n. The reference mirror is slightly tilted to facilitate the spatial carrier technique to extract the coherence function

$$\Gamma_n(x,z_1) = u_n(x,z_1)\cdot r_n^*(x,z_1) \tag{2}$$

from a single recorded hologram (Takeda et al., 1982). The basic idea is to record multiple digital holograms with different wavelengths λ_n and to evaluate them in combination. The holograms can be interpreted as spectral modes of a coherence function

$$\Gamma(x,z_1) = \sum_{n=1}^{N} \Gamma_n(x,z_1), \tag{3}$$

which can be used to numerically calculate the result of a measurement with short coherent illumination, where the coherence length depends on the bandwidth. The coherence function, given by Equation 3, will be maximum for light reflected by parts of the object that share the same optical path to the camera like the reference wave reflected by the mirror. However, in order to determine those object parts, we have to propagate the entire coherence function into the object plane z_2, i.e., calculate the spectral modes $\Gamma_n(x,z_2)$ from the recorded $\Gamma_n(x,z_1)$. This process involves the determination of both, the propagated object wave $u(x,z_2)$ and the propagated reference wave $r(x,z_2)$ and therefore requires the shape of the reference wave to be known. Let us for example, assume a plane reference wave

$$r_n(x,z_1) = r_{0,n}\cdot \exp[ik(2d+a)], \tag{4}$$

with $k = 2\pi/\lambda$ and amplitude $r_{0,n}$. In this case, we can make use of the independence of r_n from x and with the help of Equation 2 find

$$\mathcal{P}_{\Delta z}\{\Gamma_n(x,z_1)\} = \mathcal{P}_{\Delta z}\{u_n(x,z_1)\}\cdot r_n^*(x,z_1) = u_n(x,z_2)\cdot r_n^*(x,z_1). \tag{5}$$

where $\mathcal{P}_{\Delta z}\{\cdots\}$ represents a propagation operator, e.g., an implementation of the angular spectrum method (Goodman, 2005), and $\Delta z = z_2 - z_1 = -(d+a)$ is the propagation distance. Using Equations 4, 5 it is straight forward to arrive at

$$\Gamma_n(x,z_2) = u_n(x,z_2)\cdot r_n^*(x,z_2) = \mathcal{P}_{\Delta z}\{\Gamma_n(x,z_1)\}\cdot \exp[-ik\Delta z]. \tag{6}$$

again, we can add the spectral modes to yield the coherence function in the object plane $z_2 = z_1 - (d+a)$

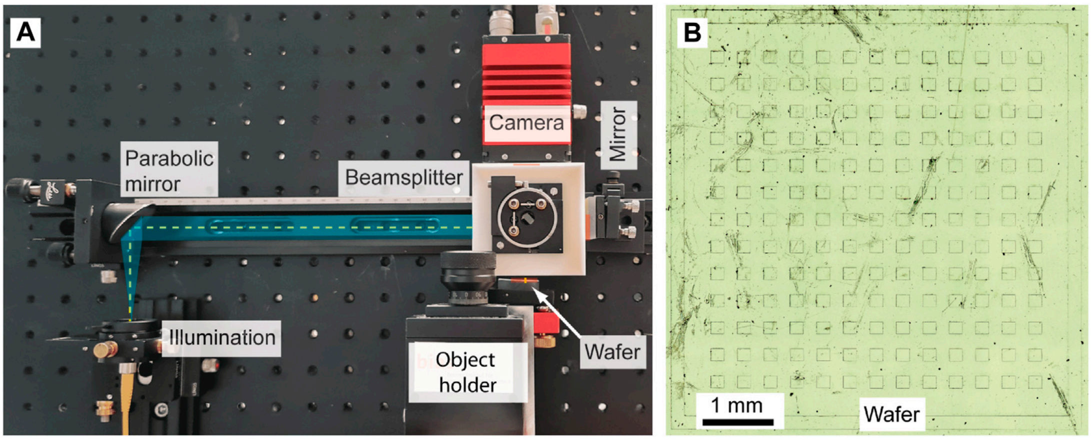

FIGURE 2
Experimental Flash-WLI setup employing spectral holography: **(A)** Photograph depicting the beam path of the Flash-WLI setup. Initially, a parabolic mirror collimates a spherical wave, which is subsequently split into object and reference waves through a 50: 50 beam splitter. The object wave illuminates the wafer surface under test (SUT), while the reference wave illuminates a flat reference mirror. The reflected light from both interferometer arms is coherently superimposed, and the resulting hologram is recorded using the camera having a pixel pitch of 4.54 μm, positioned at a distance of 81 mm from the SUT. **(B)** A bright light microscope image of the wafer test specimen consisting of a flat surface having equally spaced rectangular structures with a height of 2 μm.

$$\Gamma(x, z_2) = \sum_{n=1}^{N} \Gamma_n(x, z_2), \tag{7}$$

Equation 7 gives us a focused image of those parts of the object that have (within the limits of the coherence length) the same distance d to the beam splitter as the reference mirror.

Hence, similar to white light interferometry, the shape of the object can be retrieved by progressively changing the length of d (and thus z_2). This provides focal scanning through the object volume while evaluating the corresponding coherence function layer by layer, where large values of the coherence function indicate object points in focus. Yet, if we change d we are in principle required to move the reference mirror as well and record another set of spectral holograms to be inserted into Equation 6. However, since the reference wave is known and assumed to be a plane wave, it is not necessary to make any more measurements. Instead, we can calculate the spectral modes $\Gamma_n(x, z_1; \Delta d)$ expected from a movement Δd of the mirror by

$$\Gamma_n(x, z_1; \Delta d) = \Gamma_n(x, z_1) \cdot \exp[-ik2\Delta d], \tag{8}$$

which can be seen from replacing d by $d + \Delta d$ in Equation 4 and inserting the result into Equation 2. With Equations 7, 8, we can calculate the result of a typical coherence scanning procedure, e.g., of a WLI system, from only a single set of multi spectral holograms. From the calculated stack of coherence functions, we can then calculate the shape of the object using any evaluation method established in the field of WLI. In our case, we evaluate the real part of the calculated coherence functions and demand

$$h(\vec{x}) = \operatorname{argmax}_{z_2}[\mathcal{R}\{\Gamma(\vec{x}, z_2\}]. \tag{9}$$

In Equation 9, the height map $h(x)$ represents the shape of the surface. The great benefits of this method, when compared to standard WLI, are the very compact lensless sensor design and the significantly lower number of required recordings with just a small number of n wavelengths λ_n. The corresponding measurement systems are therefore light weight, flexible and have short acquisition times. Furthermore, because no imaging optics are involved, the method is almost immune against aberration effects allowing for a large spectral bandwidth, a tight coherence envelope, and therefore a low measurement uncertainty. Additionally, it can be made robust against mechanical vibrations through phase alignment of the spectral modes. However, the method does not come effortless, as it requires a tunable light source, additional computational demand and is limited by coherent speckle noise, because of the full spatial coherence required for the hologram recording.

Finally, to ensure a good sampling of the spectral density and optimally select the wavelengths, one needs to set $l_c = z_D$. Here, l_c denotes the coherence length of light emitted from the source and z_D is the depth of focus. Thus, the unambiguity range, Δ_r, is given by Falldorf et al. (2023).

$$\Delta_r = N \cdot l_c, \tag{10}$$

where N denotes the number of discrete lines required to perform the measurement. This means the unambiguity range, given by Equation 10, equals N times the depth of focus z_{D}.

3 Results and discussions

The experimental setup used to demonstrate the proposed method is shown in Figure 2A. This configuration is derived from the schematic shown in Figure 1. In order to achieve the modulation of the interference pattern with the spatial carrier frequency necessary for the extraction of individual coherence functions from the corresponding digital holograms, the reference mirror of the interferometer is tilted accordingly. The test object, represented by the wafer test microstructures shown in Figure 2B, is positioned at a distance of z_1 = 81 mm from the camera area. In our experiments, we used an AVT Prosilica (GT 2750)

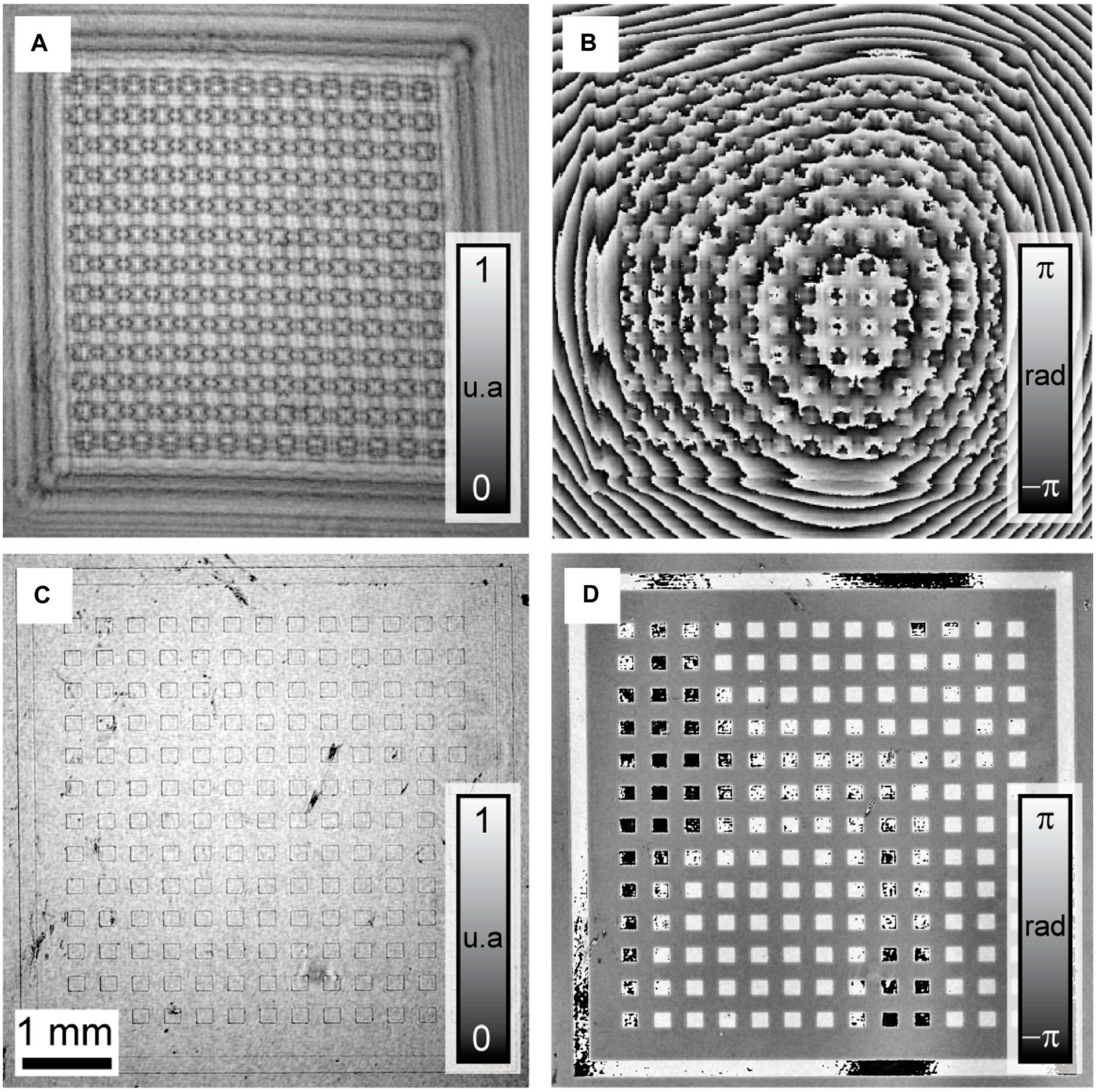

FIGURE 3
(A,B) show the amplitude and phase of a single spectral mode Γ_n in the camera plane, as obtained from the recorded hologram using the spatial carrier method; **(C,D)** show amplitude and phase of the same mode of Γ_n in the object plane, as calculated after the propagation using the plane wave decomposition.

sensor with a resolution of 2048 × 2048 pixels and a pitch of $\Delta p = 4.54$ µm in both directions. The fine structures of the wafer microstructure test object, with a height of 2 µm, were verified by examination using a standard Keyence VKX-3000 white light interferometer. This instrument is equipped with a 10× objective and a numerical aperture of 0.3, allowing comprehensive validation of the properties and dimensions of the test object.

A wavelength-tunable dye laser having a range starting from 560 nm to 615 nm served as a manually tuned light source in conjunction with a HeNe laser emitting at 632.8 nm and a solid-state laser at 488 nm, respectively, to expand the spectral width of the illumination. In the context of digital holography, the numerical aperture remains approximately constant for each object point, given by $NA \approx (2048/2) \cdot \Delta p/z_1 = 0.057$. Depending on the wavelength, the lateral resolution of the lensless sensor is approximately 6 µm.

The field of view is limited by the object side numerical aperture (the angle that the object includes with any pixel of the camera). Thus, the FOV could be simply increased by increasing the distance between the camera and the object. If the resolution shall be preserved, the number of pixels must be increased, because in this case the space-bandwidth-product of the imaging process is increased (the image provides more information).

To capture a set of data, the dye laser was manually tuned from 572 nm to 604 nm in 1 nm increments, resulting in the acquisition of 33 multi-spectral digital holograms of the wafer under test. Additionally, two holograms were captured with the

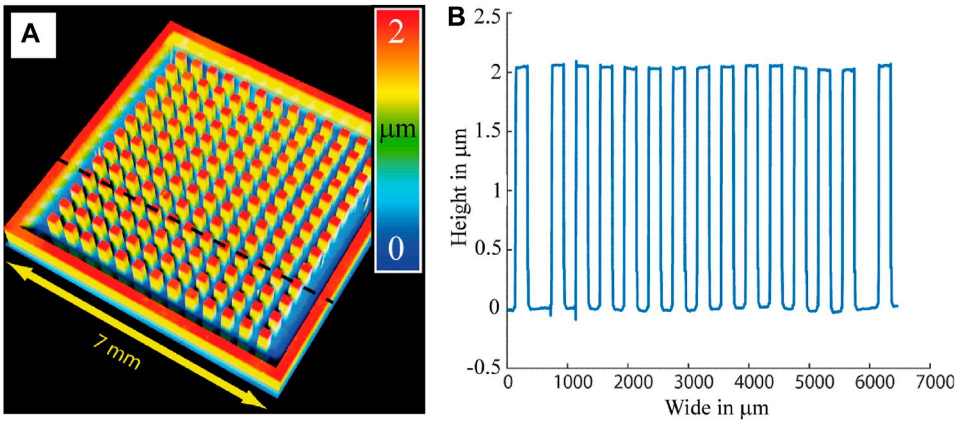

FIGURE 4
The obtained 3D profile: **(A)** A height map of the wafer microstructure, and **(B)** the profile across the dashed black line in **(A)**. The map shows square microstructures with an average height of 2.07 µm. The measurement uncertainty is $\sigma = \pm 2.5$ nm (1σ).

supplementary laser sources at 488 nm, and 632.8 nm. To calibrate the measurement system, we also captured digital holograms with a flat reference mirror placed in the object plane. The multi-spectral digital holograms of the object measurements were thus calibrated by subtracting the phase distributions of these reference measurements for every individual wavelength.

Please note that the camera exposure time is less is about 1 ms but the AVT used can only capture 20 frames per second. However, the tunable laser is manually adjusted so that each capture takes approximately 5 s. As a result, it takes about 3 min to capture all the holograms required. This time-consuming process could be improved by using a faster camera and automating the laser tuning.

However, an important result of this study is that the number of frames required for a measurement is at least one order of magnitude smaller when compared to white-light interferometers, which are often used for similar tasks.

Figures 3A, B examplarily show the amplitude and phase distributions of the complex amplitude reconstructed from the hologram captured at $\lambda = 632.8$ nm. This complex amplitude is reconstructed using the spatial carrier frequency method (Takeda et al., 1982), where the linear phase associated with the carrier frequency is removed. Subsequently, we make use of Equation 6 to propagate each spectral mode $\Gamma_n(\vec{x}, z_1)$ into the object plane, yielding $\Gamma_n(\vec{x}, z_2)$. This propagation is executed to bring the wafer background into focus. It should be noted that the precision of choosing the propagation distance is of little importance, since thereafter we select a small background area as a common reference point, where the object height is forced to be zero. This is accomplished by applying phase offsets such that the reference area maintains an average phase value of zero across each of the Γ_n. It is crucial to emphasize that this procedure is required for coupling all spectral modes and compensating for any inadvertent movements of the setup during the recording process. Figures 3C, D showcase an example of the resulting complex amplitude ($\lambda = 632.8$ nm) at that plane.

Now, applying the methodology outlined in Section 2 we calculate the coherence function along the z-axis at intervals of 10 nm. In our investigation, we specifically compute the coherence function at 3,000 depths, each separated by 10 nm. Figure 4A displays a height map of the test wafer, revealing a well-reconstructed surface across its entire axial extent. In Figure 4B, a line profile along the black dashed line is presented. The measurements indicate that the square microstructures exhibit a height of 2.07 µm, consistent with values obtained using the standard WLI model integrated into the Keyence VKX-3000.

An analysis of the local surface fluctuations across flat areas of the wafer reveals a deviation of ± 2.5 nm (1σ), closely aligned with the known production-related surface deviations of flat wafers. The results in Figure 4 demonstrate the potential of the proposed lensless multi-spectral digital holographic sensor. We required a set of only 35 recorded interferograms, to accurately measure the wafer microstructures with nanometre precision.

4 Conclusion

In this work, we have investigated the principles, implementation details and performance of the lensless multi-spectral digital holographic sensor, i.e., Flash-WLI, and demonstrated its potential in the field of semiconductor manufacturing. The method is based on the acquisition of digital holograms captured at different wavelengths. These holograms are then used to evaluate the shape of a reflective test object. Unlike WLI, Flash WLI is a lensless, robust and compact design that overcomes the limitations associated with conventional optical inspection methods such as lens-based WLI, including high requirements for mechanical vibration and bulky and heavy imaging configurations.

The experimental results, derived from the examination of a wafer sample, serve to demonstrate the effectiveness of the sensor in providing high accuracy measurements. The reported measurement uncertainty of ± 2.5 nm (equivalent to 1σ) demonstrates the accuracy of the sensor's measurements. In particular, this value agrees well with the height measurement of 2 µm obtained by the WLI model performed by the Keyence VKX-3000. This agreement not only confirms the reliability of the sensor's measurements but also underlines its consistency with established techniques, thereby increasing its integrity in the field of microstructure analysis. This level of accuracy positions the sensor as a reliable and highly accurate tool for microstructure analysis in semiconductor manufacturing.

The successful application of the sensor in semiconductor manufacturing is a significant step forward, paving the way for improved microstructure analysis and quality control in wafer manufacturing.

Data availability statement

The raw data supporting the conclusions of this article will be made available by the authors, without undue reservation.

Author contributions

MA: Conceptualization, Data curation, Investigation, Methodology, Validation, Visualization, Writing–original draft, Writing–review and editing. FT: Data curation, Investigation, Methodology, Validation, Writing–original draft. AM: Data curation, Investigation, Visualization, Writing–original draft. RB: Funding acquisition, Supervision, Writing–review and editing. CF: Conceptualization, Formal Analysis, Investigation, Methodology, Supervision, Validation, Writing–original draft, Writing–review and editing.

Funding

The author(s) declare that financial support was received for the research, authorship, and/or publication of this article. The authors are grateful to the State of Bremen for funding of this work through the program “Forschung, Entwicklung und Innovation” (FEI) within the frame of the project “Linsenlose Mikroskopie für die industrielle Qualitätskontrolle” (LiM-Q), project no. FUE0665B and to the Deutsche Forschungsgemeinsdchaft (DFG) for funding parts of the work in the context of the project “Shape measurement by means of imaging using partially coherent illumination” (Spice II), project no. 284158589.

Acknowledgments

The authors are grateful to Reiner Klattenhoff for technical support with the setup and the image acquisition system.

Conflict of interest

The authors declare that the research was conducted in the absence of any commercial or financial relationships that could be construed as a potential conflict of interest.

Publisher’s note

All claims expressed in this article are solely those of the authors and do not necessarily represent those of their affiliated organizations, or those of the publisher, the editors and the reviewers. Any product that may be evaluated in this article, or claim that may be made by its manufacturer, is not guaranteed or endorsed by the publisher.

References

Agour, M., Riemer, O., Flosky, C., Meier, A., Bergmann, R. B., and Falldorf, C. (2015). Quantitative phase contrast imaging of microinjection molded parts using computational shear interferometry. *IEEE Trans. Ind. Inf.* 12, 1623–1630. doi:10.1109/tii.2015.2481704

Bechtler, L., and Velidandla, V. (2003). Optical surface analysis: a new technique for the inspection and metrology of optoelectronic films and wafers. *Integr. Opt. Devices Fabr. Test.* 4944, 109–116. doi:10.1117/12.468295

Bergmann, R. B., Kalms, M., and Falldorf, C. (2021). Optical in-process measurement: concepts for precise, fast and robust optical metrology for complex measurement situations. *Appl. Sci.* 11, 10533. doi:10.3390/app112210533

Colonna de Lega, X., and De Groot, P. (2005). “Optical topography measurement of patterned wafers,” in *AIP conference proceedings* (American Institute of Physics), 788, 432–436.

De Groot, P., and Deck, L. (1995). Surface profiling by analysis of white-light interferograms in the spatial frequency domain. *J. Mod. Opt.* 42, 389–401. doi:10.1080/09500349514550341

Falldorf, C., Thiemicke, F., Müller, A. F., Agour, M., and Bergmann, R. B. (2023). Flash-profilometry: fullfield lensless acquisition of spectral holograms for coherence scanning profilometry. *Opt. Express* 31, 27494–27507. doi:10.1364/oe.493711

Goodman, J. W. (2005). *Introduction to fourier optics*. Englewood, CO: Roberts and Company publishers.

Krauter, J., Gronle, M., and Osten, W. (2017). Optical inspection of hidden mems structures. *Opt. Meas. Syst. Ind. Insp. X* 10329, 272–280. doi:10.1117/12.2269499

Migukin, A., Agour, M., and Katkovnik, V. (2013). Phase retrieval in 4f optical system: background compensation and sparse regularization of object with binary amplitude. *Appl. Opt.* 52, A269–A280. doi:10.1364/ao.52.00a269

Osten, W. (2018). *Optical inspection of microsystems*. Boca Raton, FL: CRC Press.

Schnars, U., Falldorf, C., Watson, J., and Jüptner, W. (2015). *Digital holography and wavefront sensing*. 2 edn. Berlin Heidelberg: Springer-Verlag.

Strapacova, T., Priewald, R., Jerman, T., and Mentin, C. (2017). “Inline wafer edge inspection system for yield enhancement of thin wafers,” in *2017 28th annual SEMI advanced semiconductor manufacturing conference (ASMC)* (IEEE), 138–143.

Takeda, M., Ina, H., and Kobayashi, S. (1982). Fourier-transform method of fringe-pattern analysis for computer-based topography and interferometry. *JosA* 72, 156–160. doi:10.1364/josa.72.000156

Vogel, M., Yang, Z., Kessel, A., Kranitzky, C., Faber, C., and Häusler, G. (2011). Structured-illumination microscopy on technical surfaces: 3d metrology with nanometer sensitivity. *Opt. Meas. Syst. Ind. Insp. VII* 8082, 245–250. doi:10.1117/12.889428